European Journal of Pharmaceutical Sciences 113 (2018) 171–184

Contents lists available at ScienceDirect

European Journal of Pharmaceutical Sciences

journal homepage: www.elsevier.com/locate/ejps

Coupled *in silico* platform: Computational fluid dynamics (CFD) and physiologically-based pharmacokinetic (PBPK) modelling

Aleksandra Vulović[a,b], Tijana Šušteršič[a,b], Sandra Cvijić[c,*], Svetlana Ibrić[c], Nenad Filipović[a,b]

[a] Faculty of Engineering, University of Kragujevac, Sestre Janjić 6, Kragujevac, Serbia
[b] BioIRC, Bioengineering Research and Development Center, Prvoslava Stojanovica 6, Kragujevac, Serbia
[c] Department of Pharmaceutical Technology and Cosmetology, University of Belgrade-Faculty of Pharmacy, Vojvode Stepe 450, Belgrade, Serbia

ARTICLE INFO

Keywords:
Computational fluid dynamics
Discrete phase modelling
Physiologically-based pharmacokinetic modelling
Amiloride
Dry powder inhaler
Particle size distribution

ABSTRACT

One of the critical components of the respiratory drug delivery is the manner in which the inhaled aerosol is deposited in respiratory tract compartments. Depending on formulation properties, device characteristics and breathing pattern, only a certain fraction of the dose will reach the target site in the lungs, while the rest of the drug will deposit in the inhalation device or in the mouth–throat region. The aim of this study was to link the Computational fluid dynamics (CFD) with physiologically-based pharmacokinetic (PBPK) modelling in order to predict aerolisolization of different dry powder formulations, and estimate concomitant *in vivo* deposition and absorption of amiloride hydrochloride. Drug physicochemical properties were experimentally determined and used as inputs for the CFD simulations of particle flow in the generated 3D geometric model of Aerolizer® dry powder inhaler (DPI). CFD simulations were used to simulate air flow through Aerolizer® inhaler and Discrete Phase Method (DPM) was used to simulate aerosol particles deposition within the fluid domain. The simulated values for the percent emitted dose were comparable to the values obtained using Andersen cascade impactor (ACI). However, CFD predictions indicated that aerosolized DPI have smaller particle size and narrower size distribution than assumed based on ACI measurements. Comparison with the literature *in vivo* data revealed that the constructed drug-specific PBPK model was able to capture amiloride absorption pattern following oral and inhalation administration. The PBPK simulation results, based on the CFD generated particle distribution data as input, illustrated the influence of formulation properties on the expected drug plasma concentration profiles. The model also predicted the influence of potential changes in physiological parameters on the extent of inhaled amiloride absorption. Overall, this study demonstrated the potential of the combined CFD-PBPK approach to model inhaled drug bioperformance, and suggested that CFD generated results might serve as input for the prediction of drug deposition pattern *in vivo*.

1. Introduction

Formulation of inhaled medicines is rather challenging, as a number of factors influence quality and efficacy of the final product. Changes in physiological parameters between individuals or population groups further impede prediction of drug product bioperformance based on drug and formulation characteristics. In order to accelerate the development of safer and more effective patient-tailored inhaled medicines and reduce the number of *in vivo* studies, formulation science needs to embrace new methods for the evaluation of drugs/dosage forms, and focus on model-based development of inhaled products. In this context, *in silico* predictive tools can facilitate rational design of inhaled pharmaceutics, which is in accordance with the Quality by Design (QbD) paradigm in pharmaceutical development, incorporated in ICH Q8(R2) guidance (ICH, 2005). Computational models and advanced simulation tools can upgrade our understanding of the complex physiological processes, and interactions a drug goes after inhalation, and thus facilitate the development of inhalation medicines.

1.1. Computational fluid dynamic (CFD) analysis and discrete phase modelling (DPM)

Technology development, such as computer power becoming cheaper and available software more powerful, led to increased use of computer-based simulation in different branches of science and engineering (Wong et al., 2012).

* Corresponding author at: Department of Pharmaceutical Technology and Cosmetology, University of Belgrade — Faculty of Pharmacy, Vojvode Stepe 450, 11221 Belgrade, Serbia.
E-mail addresses: aleksandra.vulovic@kg.ac.rs (A. Vulović), tijanas@kg.ac.rs (T. Šušteršič), gsandra@pharmacy.bg.ac.rs (S. Cvijić), ibric@pharmacy.bg.ac.rs (S. Ibrić), fica@kg.ac.rs (N. Filipović).

http://dx.doi.org/10.1016/j.ejps.2017.10.022
Received 1 June 2017; Received in revised form 11 October 2017; Accepted 14 October 2017
Available online 17 October 2017
0928-0987/

Dry powder inhalers (DPIs) deliver drugs in the form of a dry powder. Aerosol particles that are generated by this type of inhalers show good results and offer advantages such as fast delivery of particles to the lungs (Clark, 2004; Chan, 2006). DPIs do not require use of propellants, they lead to higher deposition of aerosol particles within the lungs and also simplify the inhalation technique. DPIs help to reduce the fluctuation of the inhaled dose compared to other available inhalers such as Metered Dose Inhalers (Brocklebank et al., 2001; Terzano, 2008) as well as reduce systemic side effects compared to other drug delivery routes (Hoppentocht et al., 2014). The problem with these devices is their inefficiency, since < 30% of dose reaches the lungs (Islam and Gladki, 2008). In order to improve the performance of these inhalers we need to understand the dispersion and deposition mechanisms better.

Computational fluid dynamics (CFD) can be used for modelling both laminar and turbulent flow (Wong et al., 2012). The disadvantages of the CFD approach are that it can only simulate airflow and it is not possible to consider particle interaction. The advancement in the field of CFD analysis has created a possibility for a new approach for inhalator modelling. This advancement allowed for aerosol transport and deposition to be calculated in realistic three-dimensional (3-D) models of the inhaler (Longest and Holbrook, 2012).

Several computational fluid-particle dynamics (CF-PD) models are available for the calculation of air-drug mixture dynamics (Feng and Kleinstreuer, 2014), such as the discrete phase model (DPM), two-fluid model, mixture model, dense dispersed phase model (DDPM), and the discrete element method (DEM) (Kleinstreuer et al., 2014). In order to gain knowledge on particle dispersion we need to couple CFD with DPM. Some authors investigated commercial DPIs using CFD-DPM analysis in order to gain better knowledge on dispersion mechanisms. Zhou et al. (2013) researched the effect of device design of the commercial DPI, the Aerolizer® on the aerosolization of a carrier-based DPI formulation (Foradile®) using a combination of CFD and DPM, while Jiang et al. (2012) using the same method investigated the effect of powder residence time on the performance of the Aerolizer DPI. CFD coupled with experimental powder dispersion analysis, can provide an initial quantification of the turbulence levels and average particle impaction velocities. This information can help maximize the dispersion performance of a DPI (Coates et al., 2006).

The findings presented by Mossaad (2014) suggest that the deposition profile of inhalation dry powders is affected by two major independent factors:

(1) patient-related factors; which can be cited as the anatomical and physiological aspects of the respiratory system as well as the inhalation airflow rate;
(2) physical properties of dry powder formulations; which include properties of pure drug as well as properties of nanocarrier systems.

Most marketed DPIs are passive inhalers that employ the patient's inspiratory effort to generate the necessary airflow, and the associated turbulence, to overcome the cohesive nature of the respirable active pharmaceutical ingredient (API) and fluidize the powder bed into a respirable aerosol (Wong et al., 2012). Voss and Finlay (2002) investigated the effect that air turbulence has on the *in vitro* DPI performance.

Coates and co-workers have analyzed the effect of the Aerolizer® design on device performance. They have analyzed the influence of airflow (Coates et al., 2005a), grid structure and mouthpiece length (Coates et al., 2004), mouthpiece geometry (Coates et al., 2007), inlet size (Coates et al., 2006) as well as the role of the capsule (Coates et al., 2005b). They have found that:

- increased flow rate through the Aerolizer® leads to increased level of turbulence (Coates et al., 2005a);
- the grid straightens the airflow exiting the device, and increase in grid voidage leads to the increase of the amount of mouthpiece retention (Coates et al., 2004);
- the length of the mouthpiece has no significant effect on the performance of the device (Coates et al., 2004);
- widening of the Aerolizer® exit makes a small difference to the dispersion performance, and it reduces the axial velocity of the exiting airflow which leads to reduced throat impaction (Coates et al., 2007);
- the air inlet size reduction leads to increased turbulence and particle impaction velocities within the device at low flow rates, which enhance the dispersion performance (Coates et al., 2006);
- the capsule reduced the turbulence levels within the device, while its size does not have significant effect on performance (Coates et al., 2005b).

Information obtained using computer based simulation (CFD and DPM analysis) help us understand dispersion mechanisms better. This knowledge can be used for inhaler design changes in order to create more efficient device.

1.2. Physiologically-based pharmacokinetic (PBPK) modelling

Physiologically-based pharmacokinetic (PBPK) modelling is a relatively new concept pointed out to be beneficial for the *in silico* simulation of drug pharmacokinetic behavior following drug administration through different dosing sites. In comparison to simpler compartmental pharmacokinetic models, which have no physiological meaning, PBPK models forecast drug pharmacokinetics as a function of physiology characteristics (Bouzom et al., 2012; Jones and Rowland-Yeo, 2013). These properties may change in disease states or due to inter- or intra-subject variations, and if the relevant physiological properties are known, PBPK model can be used to predict drug pharmacokinetics in target population or tailor drug dosing for the purpose of personalized therapy (Suri et al., 2015; Almukainzi et al., 2016). In addition, PBPK models can provide mechanistic explanation for unusual or unexpected data observed *in vivo* (Peters, 2008; Samant et al., 2017). Another advantage of PBPK models is that they can serve as a basis for the prediction of drug-drug interactions (Zhou et al., 2016; Zhuang and Lu, 2016), which is of particular importance for poly-medicated patients. There have also been attempts to link PBPK models with drug pharmacodynamic properties, and predict drug exposure and pharmacodynamic effect (Chetty et al., 2014; Alqahtani and Kaddoumi, 2016).

Most efforts have been directed to the development of predictive PBPK models for orally administered drugs, while mechanistic PBPK models for other dosing routes are relatively new, and still poorly exploited. There are several software tools for PBPK modelling of inhaled drug absorption (Borghardt et al., 2015; Fröhlich et al., 2016). Among these is GastroPlus™ software package, with the integrated Pulmonary Compartmental Absorption & Transit (PCAT™) model able to predict the absorption and disposition of drugs administered *via* intranasal and/or respiratory route. Modelling and simulation with this software can be used to assess the influence of drug properties, drug dose and/or dosage form characteristics on drug *in vivo* absorption/disposition, as well as to mechanistically interpret the influence of different physiological or disease related factors on drug absorption. However, published examples of the application of PCAT™ model are still scarce (Wu et al., 2013; Backman et al., 2016; Wu et al., 2016).

One of the critical factors affecting the reliability of the PBPK modelling results is the selection of input data that characterize dosage form properties, such as size distribution of particles leaving the inhaler. Common methods to assess aerodynamic properties of aerosolized particles rely on *in vitro* tests using impingers or impactors (Mitchell and Nagel, 2003). These methods are predominantly designed to provide data on lung particle deposition, and they are used for the *in vitro* assessment of inhaled drugs bioequivalence. However, there are certain issues about the accuracy of these methods (de Boer et al.,

2002), and the obtained results (expressed as mass median aerodynamic diameter (MMAD), and geometric standard deviation (GSD)) might not necessarily reflect actual aerosolized particle size distribution (PSD). As an alternative to the *in vitro* determination of MMAD and GSD, CFD simulations may provide data on PSD, which can further be used as input for the calculation of deposition fractions in different lung compartments.

The purpose of this study was (i) to link the CFD simulations of particle distribution from DPI with PBPK modelling in order to predict *in vivo* deposition and absorption of the inhaled model drug, amiloride hydrochloride. The additional goals were (ii) to compare CFD simulation result with the *in vitro* data obtained using Andersen cascade impactor (ACI), and (iii) to mechanistically interpret the influence of formulation properties and physiological factors on amiloride deposition and absorption following inhalation.

Amiloride is a sodium channel blocker with weak diuretic properties, commonly used to treat oedema associated with hepatic cirrhosis and heart failure. Amiloride, as hydrochloride (HCl) salt, has also been used in the management of cystic fibrosis, due to its ability to reduce sodium and water absorption from the lung luminal membrane and preserve airway surface liquid. Inhaled amiloride acts locally in the bronchiolar airway epithelium, but if absorbed in large percent, high plasma concentrations may cause hyperkalemia and undesirable cardiovascular effects (Jones et al., 1997). Therefore, it is important to understand the disposition and plasma concentration-time profile following inhalation of this drug.

2. Materials and methods

2.1. Drug physicochemical and aerodynamic properties

Drug-related input parameters required for CFD and PBPK simulations were experimental data taken from literature or *in silico* estimated values. The selected data and appropriate references are denoted in the relevant sections.

Physicochemical and aerodynamic properties of the model amiloride HCl DPI formulations were previously determined *in vitro* as described in the study of Djokic et al. (2014). Four jet-milled samples (JM1-JM4) were prepared under different experimental setups, with varying three jet-milling process variables (*i.e.* diameter of injector nozzle for injectable air, diameter of ring nozzle for grinding air, and air pressure for milling). The fifth sample (SD) included respirable spray-dried amiloride HCl particles prepared from aqueous feed solutions under controlled conditions (feed concentration, feed rate, atomization pressure, inlet temperature, outlet temperature) to obtain size distribution comparable with jet-milled particles. The key properties of the obtained samples relevant for CFD-DPM simulations of DPI performance (*i.e.*, geometric particle size expressed as d_{10}, d_{50}, d_{90}, powder density) are depicted in Table 1. Geometric PSDs were determined by laser diffraction, and true density of the samples was measured using helium pycnometry. Djokic et al. (2014) also examined aerosol

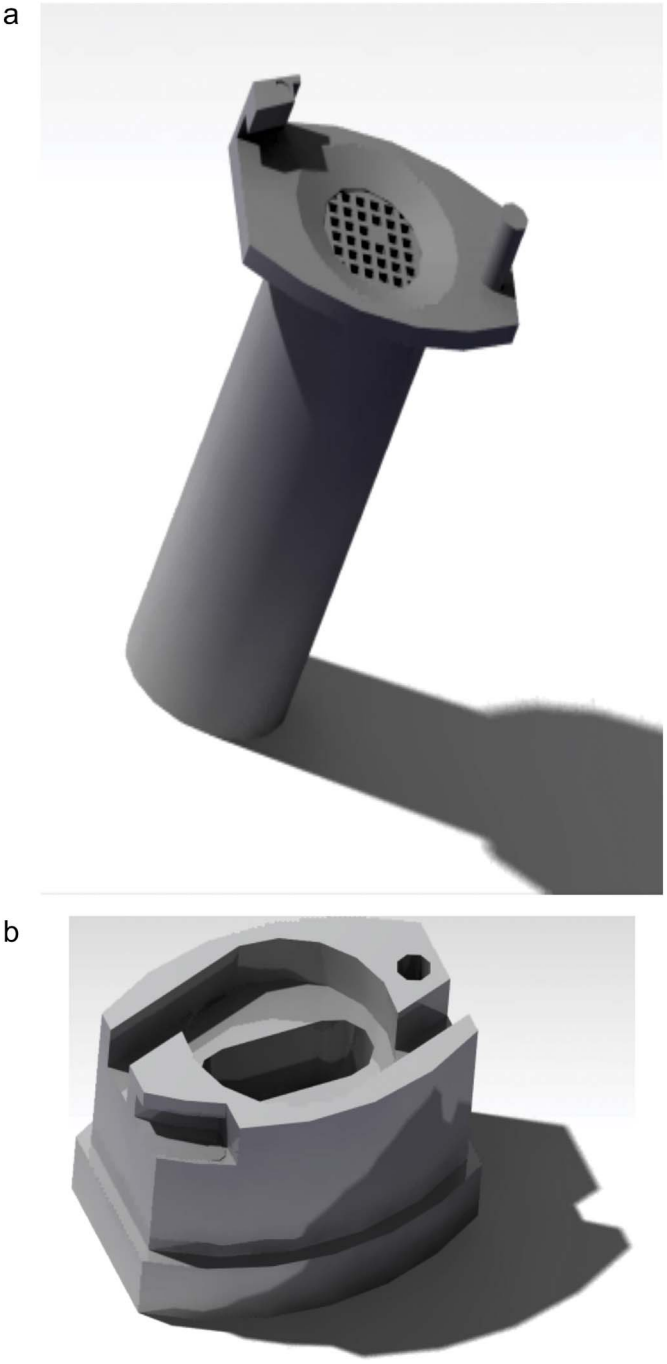

Fig. 1. Created model – solid domain: mouthpiece with grid area (a) and base with capsule storage (b).

Table 1
Physicochemical and aerodynamic properties of amiloride HCl DPI samples[a].

Sample	d_{10}; d_{50}; d_{90}[b] (μm)	True density (g/cm^3)	ED[c,e] (%; mg)	FPF[d,e] (%)	MMAD[e] (μm)	GSD[e]
JM1	0.84; 1.71; 4.01	1.67	68.15; 13.63	39.78	7.30	2.74
JM2	0.80; 2.07; 4.92	1.68	70.54; 14.11	41.25	7.27	2.37
JM3	0.87; 2.62; 6.58	1.72	82.97; 16.59	45.67	5.53	1.68
JM4	0.86; 2.96; 7.31	1.73	84.23; 16.85	50.62	5.71	1.51
SD	0.85; 2.89; 7.16	1.71	83.74; 16.75	50.19	5.61	1.58

[a] Taken from (Djokic et al., 2014).
[b] Intercepts (geometric particle size) for 10%, 50% and 90% of the cumulative particle mass.
[c] ED – emitted dose (percentage/mass of particles delivered from the inhaler).
[d] FPF – fine particle fraction (percentage of the mass of drug particles that have aerodynamic diameter of < 5 μm).
[e] These values were not used as inputs for the simulations.

dispersion characteristics with eight-stages ACI with a pre-separator using the Aerolizer® (Pfizer) DPI device filled with 20 mg drug. Methods of determination are described in detail in the published study (Djokic et al., 2014). Relevant parameters calculated based on ACI measurements (*i.e.* emitted dose (ED), fine particle fraction (FPF), MMAD and GSD values) are also depicted in Table 1. These data were used for comparison with the values estimated based on the CFD-DPM results.

2.2. CFD simulations

2.2.1. 3D geometric models

In order to simulate powder dispersion in a commercial inhaler, three-dimensional model of DPI had to be made. Aerolizer® model was created using commercial software for computer aided design based on the geometry of the Aerolizer® device (Fig. 1) which was constructed from detailed measurements taken from the marketed device using a micrometer. Some simple model modifications were added in order to remove chamfered and curved edges. These edges were ignored in areas where that do not have any effect on the process of inhalation. From this model we have taken the inner cylinder and inner compartment where air and drug particles flow (fluid domain). This fluid domain model (Fig. 2) consists of a chamber with two inlets, a barrel, a grid in between and a capsule for powder storage. This model was exported as .stp file that was later used for mesh creation and to define boundary conditions. Meshed model is shown in Fig. 3. Unstructured (tetrahedral) mesh was used. The tetrahedral cells were then converted to polyhedral cells to reduce the skewness of the overall cell count. The model grid consists of 281,782 polyhedral cells and 1,402,608 nodes. The grid was refined in the areas with expected large gradients of flow and then additionally refined near the wall based on the initial solutions.

2.2.2. Numerical simulation

In order to precisely describe what happens during inhalation in the device and in large airways we need to use turbulent flow. The commercial CFD software ANSYS Fluent 16.0 was used to simulate fluid flow which is governed by the Navier–Stokes equations:

$$\rho\left(\frac{\partial v_i}{\partial t} + v_j\frac{\partial v_i}{\partial x_j}\right) = -\frac{\partial p}{\partial x_i} + \mu\left(\frac{\partial^2 v_i}{\partial x_j \partial x_j} + \frac{\partial^2 v_j}{\partial x_j \partial x_i}\right) \quad (1)$$

The boundary conditions of air inlets, outlet of mouthpiece and other walls in the computational models were set as velocity inlet, outflow and wall, respectively. To simplify conditions in the model, it was assumed that:

(1) air in the model was incompressible;
(2) flow in the inlets was steady and normal to the surface area of the inlet;
(3) the friction heat was negligible in this process.

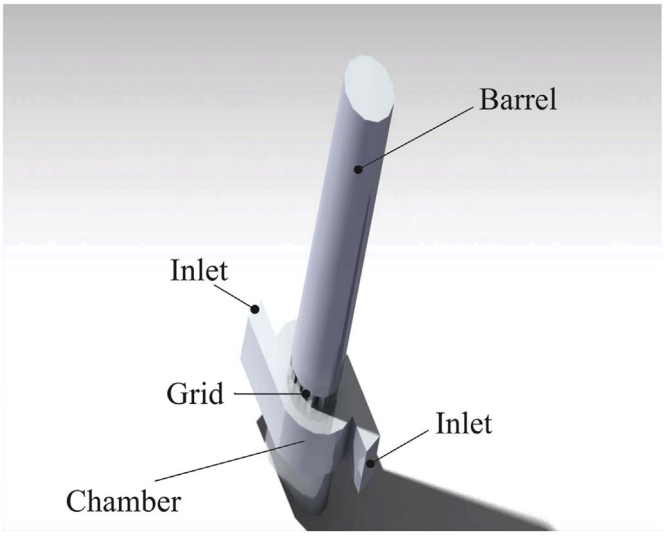

Fig. 2. Created three-dimensional – fluid domain.

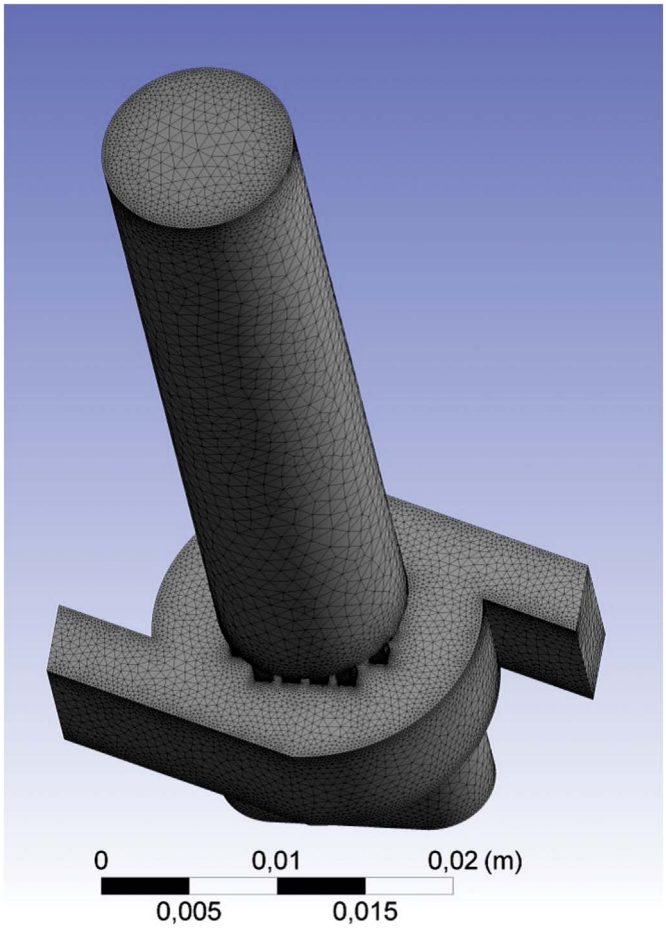

Fig. 3. Meshed model.

According to Milenkovic et al. (2013), during forced inhalation the instantaneous volumetric flow rate rapidly increases and reaches its highest value. This instantaneous flow rate is approximately equal to the highest value during inhalation and this leads to the possibility to approximate dynamic airflow as steady airflow which was done here.

In general, the k-ε model or the k-ω model can be used for inhalation problems. Launder and Spalding (1974) as well as Menter (1994) have provided more details on these turbulence models. Many researchers have used the k-ω or Menter's Shear Stress Transport (SST) models. Versteeg et al. (2000), Longest et al. (2007), Kleinstreuer et al. (2007), Longest et al. (2008), Longest et al. (2009) have used this model because of its capability to be applied throughout the turbulent boundary layer. Therefore, Standard k-ω model with low Reynolds number (LRN) was adopted for the turbulent flow of air as fluid. The k-ω turbulent model is a two-transport-equation model for turbulence prediction based on two partial difference equation for two variables (kinetic energy k and specific turbulent dissipation rate or turbulent frequency ω). This model has shown good accuracy when combined with high efficiency in comparison to complex methods, such as large eddy simulation (LES) (Longest et al., 2013). The LRN k-ω model can be used for accurate prediction of pressure drop, velocity profiles, and shear stress for transitional and turbulent flows (Ghalichi et al., 1998).

All transport equations were discretized to be at least second order accurate in space. A Second-Order Upwind scheme was used to discretize the pressure equations, and a Quadratic Upwind Interpolation for Convection Kinetics scheme was used to discretize the momentum and turbulence equations. Both of these schemes provide second-order accuracy (Shur et al., 2012). The numerical equations were converged to a steady-state solution. Rosin-Rammler diameter distribution of inert particles, injected using face normal direction, was used as input for Fluent's Discrete Phase Model (DPM). Collisions of particles with the DPI walls occur predominantly due to inertial impaction. The particle-wall collision frequency and capture efficiency, which determine the rate of deposition, are controlled by adhesion forces (Milenkovic et al., 2014a). We simulated the case when powder instantaneously breaks-up into a population of particles and aggregates identical to that of the free-flowing powder after which no more breakage or aggregation occurs. Although this approach represents a limiting case of weak cohesion forces, it provides a means for evaluating the effects of flow rate, particle size, and adhesion forces on the local and total particle deposition in the DPI device. With DPM, each particle is presented by a parcel of particles and this method neglects inter-particle collisions (Kloss et al., 2009). Due to the number of different simulations performed, it was not feasible to use additional tools such as Discrete Element Method (DEM), which considers collision breakage or particle – particle collision. This approach needs greater CPU effort (Kloss et al., 2009) and will be left for future work.

It was assumed that particles behave in such way that in contact with wall they stay “trapped” and the particles that reach the outlet surface “escape” the device domain. This assumption is valid due to the fact that normal component of the particle velocity at the moment of impact with the inhaler wall (v_n) is smaller than the critical normal velocity throughout the simulation (v_c). Detailed impaction model calculation can be found in Milenkovic et al., 2013.

In that way, it could be calculated how many particles were set at the beginning of the calculation and how many particles got out of the device.

In order to solve the particle trajectories the spherical nonlinear drag law implemented in ANSYS Fluent (version 6.3, ANSYS, USA) was used. For a low Reynolds number, mentioned law reduces to Stokesian drag law. The gravitational acceleration was not included throughout the simulations. It was shown that the gravity has the insignificant impact due to small aerosol diameter sizes and short residence times in the inhaler itself (Milenkovic et al., 2013). It is assumed that all particles were released at the same time (beginning of simulation) using Rosin-Rammler distribution on the inlet surface. Particle size is considered to be constant throughout simulation. In general, particle cohesion forces affect the initial powder release and dispersion dynamics as well as aggregate deposition and breakage, as observed and explained in Milenkovic et al. (2014b). Interactions between particle or aggregate with the inhaler walls, other particles or aggregates is very important. Outcome of these interactions is breakage of aggregates into smaller aggregates and fine particles which are important as they are best suited to target the upper respiratory tract (Milenkovic et al., 2013; Milenkovic et al., 2014b). Boundary conditions for this simulation included velocity at the two inlets and pressure outlet (underpressure to simulate suction effect which comes from the inhalation). The normalized Reynolds stress residuals in the range of $10e^{-4}$ were applied as the convergence criteria to ensure full convergence. Inlet velocity was calculated from the flow rate (28.3 l/min) and it was 11.79 m/s. This flow rate was used because the aerodynamic PSD was experimentally measured at this airflow rate (Djokic et al., 2014). Particle mass at the beginning was 20 mg. In total 5 simulations were performed, 4 for jet-milled particles (JM1, JM2, JM3 and JM4) and 1 for spray-dried particles (SD). Diameter and density values used for these simulations are given in Table 1.

2.3. Aerodynamic particle size distribution of CFD-DPM generated aerosol particles

The results of CFD-DPM numerical simulations for the five model formulations, namely geometric diameter, density and mass of the particles leaving the inhaler, were used to quantify aerodynamic PSDs of the generated aerosol by calculating the corresponding MMAD and GSD values. Aerodynamic particle diameter ($d_{aerodynamic}$) was calculated from the following expression:

$$d_{aerodynamic} = d_{geometric} \times \sqrt{\rho} \quad (2)$$

where $d_{geometric}$ and ρ are geometric particle diameter and particle density, respectively. MMAD for each sample (JM1, JM2, JM3, JM4 and SD) was estimated from the plot representing percentage cumulative mass *vs.* cut-off aerodynamic diameter on a log-scale. The applied method was based on linear interpolation between the nearest data points on either side of the cumulative 50th mass percentile value (Christopher et al., 2010). GSD was derived from the estimated d_{16} and d_{84} for each sample using the Eq. (3):

$$GSD = \sqrt{\frac{d_{84}}{d_{16}}} \quad (3)$$

where d_{16} and d_{84} are aerodynamic particle diameters at the 16th and 84th cumulative mass percentiles. The estimated MMAD and GSD values based on CFD-DPM data, along with the CFD-DPM predicted ED, were further used as inputs in the designed amiloride-specific PBPK model, to explore model estimates on drug deposition and absorption in the lungs following inhalation of the five model formulations.

2.4. Drug-specific PBPK model

Amiloride absorption and concomitant pharmacokinetic processes following oral and inhalation administration were simulated using GastroPlus™ software (version 9.0.0007, SimulationPlus Inc., USA). The *in silico* study consisted of two phases: first model construction, and afterwards model exploration. The first phase referred to the selection of input parameters and evaluation of the simulation outcomes by comparison with the data from the *in vivo* studies. In the exploration phase, the generated drug-specific PBPK model was used to forecast amiloride deposition and absorption following inhalation of the model formulations (JM1-JM4, SD).

Drug absorption was predicted using Advanced Compartmental Absorption and Transit (ACAT) fasted-state model, linked with PBPK model to simulate drug disposition through different body tissues, and PCAT™ model to account for drug bioperformance in the respiratory tract. The ACAT model of human gastrointestinal (GI) tract is comprised of nine compartments linked in series (stomach, duodenum, two jejunum compartments, three ileum compartments, caecum, and ascending colon), which are further subdivided to account for the drug that entered into the enterocytes. The effect of physiological conditions on drug absorption as it transits through successive GI compartments is managed by a series of differential equations (Agoram et al., 2001). The drug was assumed to substantially bind in enterocytes (95%), to account for the delayed time to reach maximum plasma concentration (t_{max}) (Savic et al., 2007). This phenomenon was observed in case of other basic drugs with high solubility/fast dissolution and high permeability (Sarfraz et al., 2015; Samant et al., 2017).

In extension to the ACAT model, PBPK model enabled simulation of drug distribution in major tissues linked together by blood circulation (Theil et al., 2003; Kostewicz et al., 2014). Each tissue was described by a set of physiological parameters, whereas default parameters for the selected “30 years/70 kg” physiology were generated by the software, based on population mean values obtained from published data. All of

Table 2
Summary of input parameters for PBPK simulations.

Parameter	Value
Molecular weight (g/mol)	229.63
logD (pH 7.4)	− 0.86[a]
pK_a	8.7[b]
Solubility (aq) (mg/ml)	5.2[b]
Human jejunal permeability, P_{eff} ($\times 10^{-4}$ cm/s)	1.6[c]
Diffusion coefficient ($\times 10^{-6}$ cm^2/s)	8.86[d]
Fluid intake with oral dose (ml)	250[e]
Mean precipitation time (s)	900[e]
Particle radius for oral dosing (μm)	25[e]
MMAD for the nebulized solution (μm)	4[f]
Drug particle density (g/ml)	1.2[e]
Blood/plasma concentration ratio	1[e]
Unbound percent in plasma (%)	60[g]
Body weight (kg)	70
Renal clearance, CL_{ren} (l/h)	25[h]
Unbound percent in enterocytes (%)	5[h]

[a] Taken from (Zhu et al., 2002).
[b] Taken from (IPCS INCHEM, n.d).
[c] Taken from (Dahlgren et al., 2015).
[d] GastroPlus™ predicted.
[e] GastroPlus™ default values.
[f] Taken from (Jones et al., 1997).
[g] Taken from (Spahn et al., 1987).
[h] Optimized values.

the tissues were considered to be well-stirred, and drug distribution was treated as perfusion limited. Tissue to plasma partition coefficients (Kp values) were calculated using the default Rodgers-Single (Lukacova) Kp method (Lukacova et al., 2008), and further optimized (multiplied by 3.5 scaling factor) to capture the experimental data on drug volume of distribution (Vd). Amiloride is predominantly excreted by the kidneys *via* tubular secretion, which signifies relatively high renal clearance values (approximately 3 times the creatinine clearance) (Spahn et al., 1987). The estimated value for model development of 25 l/h was in the range of values reported in literature (Spahn et al., 1987; Fagerholm, 2007; Savic et al., 2007).

In case of drug dosing *via* respiratory route, PCAT™ model was used to describe drug transit and absorption through the following pulmonary compartments: extra-thoracic (nasopharynx, oropharynx, larynx), thoracic (trachea, bronchi), bronchiolar (bronchioles, terminal bronchioles), and alveolar-interstitial (respiratory bronchioles, alveolar ducts and sacs, interstitial connective tissue) (Chaudhuri and Lukacova, 2010). Deposition of inhaled particles in each compartment was calculated by the software built-in ICRP 66 deposition model (ICRP, 1994). Nasal-pulmonary physiology parameters were kept at software default values. The additional input parameters required for the simulation were obtained from literature or *in silico* estimated (Table 2).

In the model construction phase, published data from amiloride pharmacokinetic studies were used to evaluate the generated drug PBPK model. Digital extraction of literature data from the graphs was performed using DigItTM program (version 1.0.4, Simulations Plus, Inc., USA). Amiloride-specific PBPK model for oral drug delivery was validated by comparing the simulation results with drug plasma concentration-time profiles following administration of oral solution (Jones et al., 1997), or single amiloride HCl immediate (IR)-release capsule (Weiss et al., 1969). The predictive power of the adjusted pulmonary drug delivery model was assessed by comparing the simulation outcomes with the *in vivo* data on amiloride plasma profiles following pulmonary delivery of the nebulized solution (Jones et al., 1997). In order to simulate the deposition pattern of the nebulized solution, we used *in vitro* obtained MMAD value from literature as input. We need to note that the proper way to validate the applied CFD-PBPK modelling approach would be to use CFD simulated MMAD and GSD as input values. But, due to the lack of relevant CFD data for this nebulized solution, an *in vitro* obtained MMAD was used. Another annotation regarding the construction of the PCAT™ model is that drug systemic absorption rate constants in the pulmonary compartments (Ka(p)) were varied to assess the influence of the absorption kinetics in the lungs on the generated pharmacokinetic profiles.

Predictability of the generated models (oral and inhalation) was measured by the percent prediction error (%PE) between the simulated and *in vivo* observed data:

$$\%PE = \frac{observed - predicted}{observed} \times 100 \quad (4)$$

In the model exploration phase, the constructed model was used to estimate the expected drug deposition and absorption following inhalation of five model formulations (JM1-JM4, SD). In this step, MMAD and GSD values calculated based on the aerodynamic aerosol particle distribution on the outlet of the Aerolizer® model, obtained by CFD-DPM, were used as inputs in the PBPK model. Also, CFD-DPM predicted ED for each model formulations was used to define drug dose, and drug dissolution in the lungs was predicted based on CFD predicted geometric PSD and input drug solubility.

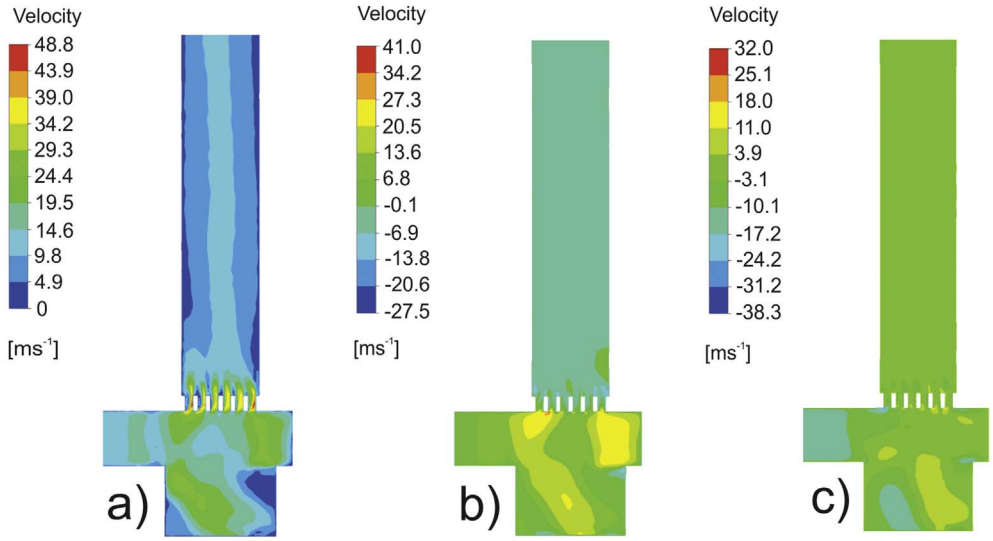

Fig. 4. Velocity contours for JM2: velocity magnitude (a), tangential velocity (b), radial velocity (c).

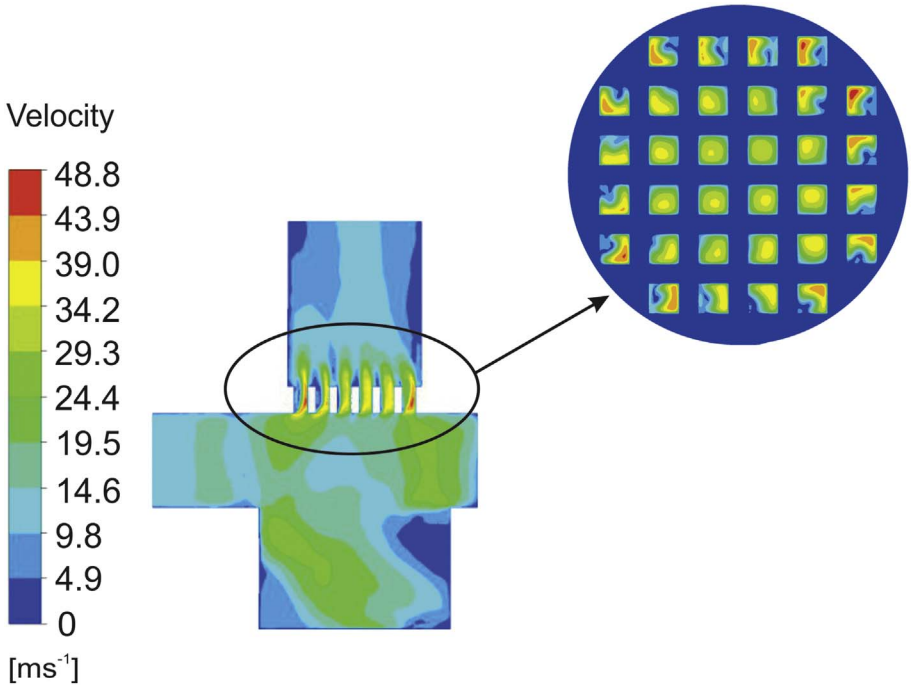

Fig. 5. Velocity distribution detail (JM2), grid area – volume rendering.

3. Results and discussion

3.1. CFD simulation results

Results for jet-milled samples and spray-dried sample are similar with small differences in peak values. In order not to repeat figures, we will only show results for JM2 sample.

Fig. 4 shows the velocity magnitudes, tangential and radial velocities for *xz* plane obtained from simulation using previously mentioned parameters. Flow pattern in the inhaler is complex, due to swirling motion inside the capsule chamber that incoming flow generates. The highest velocity is observed inside the grid, *i.e.*, about 48 m/s, while the lowest one is in the barrel. Obtained velocity values and distribution can be compared to values in other published papers (Tong et al., 2013).

Fig. 5 shows the velocity distribution in the grid area. It can be noticed that grid suppress the turbulence in the barrel and also reduces swirl that is generated in the capsule chamber. Higher air inlet velocity leads to wider impact velocity and higher turbulence levels. Presented results are similar to the results obtained by Coates et al. (2006).

Maximum velocity values are in range from 45.23 m/s (JM3 and JM4) to 48.81 m/s (JM2 and SD). Fig. 6 shows the outlet velocity vectors for jet-milled (JM1, JM2, JM3, JM4) and spray-dried particles (SD), which is helpful in determination of particles deposition in the oral cavity.

As seen in Fig. 7, the fluid flow inside the Aerolizer evokes particle collisions with the inhaler wall, especially in the area of carrier and chamber before grid structure. It should be noted that particle–particle collisions generally have to be taken into account. However, when the particle volume fraction is less than about 10^{-3} (Sommerfeld et al., 2008) this can be ignored. Therefore, due to the small volume fraction (10^{-4}) in this work, the effect of particle – particle collisions were not considered or taken into account. Most of the carrier-device collisions as well as carrier-carrier collisions occur in the chamber. Carrier-device collisions are more common than carrier-carrier collisions. This type of collision (carrier-carrier) rarely happens in the barrel because the flow in the barrel is less turbulent than the flow in the chamber and also because the particles enter the barrel at the different times and reduce the chance for collision. However, the main reason for why carrier-carrier collisions rarely occur is the very small particle volume fraction. The particle-particle collision rate depends on the second power of the local particle number density function. Studies such as Li and Ahmadi (1992), Ge et al. (2012) and Zhou et al. (2013) have used similar conditions regarding particle collision where rebound was ignored. Obtained results can be compared to the result obtained by Tong et al. (2015). This swirling flow reduces and becomes less dominant through the mouthpiece, as the tangential air inlets which introduce a swirl component, don't have such great impact down the flow after the grid structure.

3.2. Particle tracking results

The particle tracking was initially carried out to simulate the dispersion of 1000 particles and repeated for 5000, and 10,000 particles to determine if the particle impaction velocities obtained were independent of the number of particles simulated. Since the velocities proved to be independent of the number of particles, we could continue working with smaller number of particles, since the simulation time and necessary computer memory drastically increases with particle number.

Particles mostly get “trapped” inside the carrier area because of the swirl flow. This happens after a very short period, showing that the residency time in this area is short. Fig. 8 shows the results of particle tracking from all jet-milled particles as well as spray dried particles. In order to have better visualization only 20 tracks were shown. Particles at the exit of the barrel are concentrated in the middle.

3.3. Comparison of in vitro data and in silico predictions for the model DPI formulations

Comparative analysis of the *in vitro* obtained data (Djokic et al., 2014) and *in silico* CFD-DPM predictions revealed similar values for the percent ED (Fig. 9a). In the case of JM1, almost identical values were obtained *in vitro* and *in silico*. An excellent match was also seen for the other jet-milled samples (difference in ED up to 4%), whereas for spray-dried sample the obtained difference between these values was about 4.5%. Such results demonstrate that the generated DPI inhaler model adequately describes aerosolization of five model formulations, and can be used to calculate ED of an aerosolized DPI.

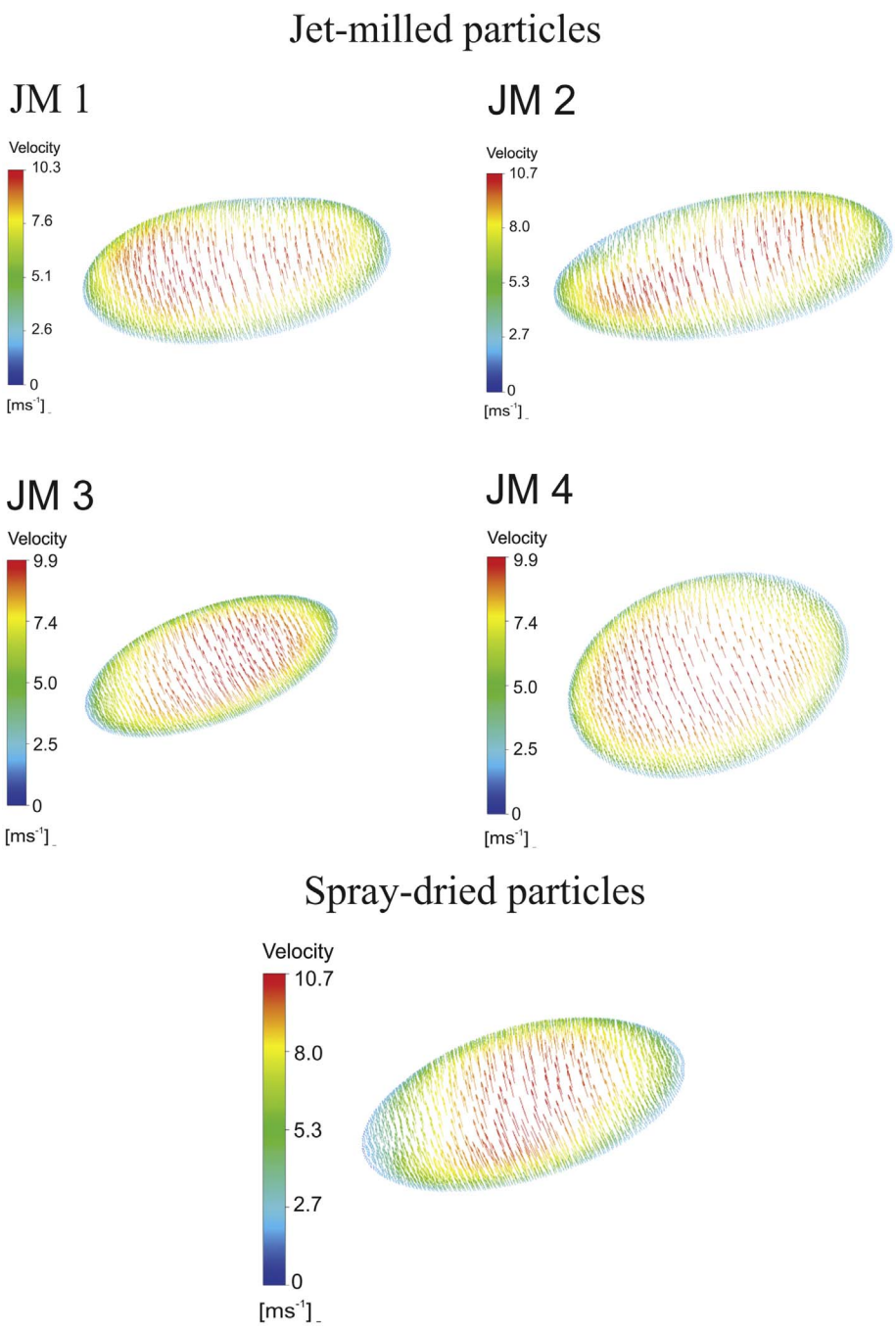

Fig. 6. Outlet velocity vectors for jet-milled and spray dried particles.

According to the simulation outcomes, the ED from all tested formulations is comprised of particles with the aerodynamic diameter of < 5 μm, and therefore can be considered as FPF. In contrast, the values resulting from ACI measurements indicate that only about 40 to 50% of the emitted particles mass correspond to FPF, depending on the formulation (Table 1). The differences in FPF values based on CFD-DPM simulations and ACI measurements may arise from the presence of agglomerates which are detected by the ACI device, in addition to the fine particle adhesion (and loss) onto inner ACI walls, while the applied *in silico* modelling follow the trajectories of single particles. This implies that both methods have certain limitations. The generated CFD-DPM model does not take into account particle agglomeration that most likely happens prior to and during aerosolization, and therefore the estimated FPF values might be overestimated. On the other hand, during ACI measurements drug particles may also agglomerate and de-agglomerate during fractionation (Strickland et al., 2013), meaning that the obtained results do not necessarily reflect just the influence of agglomerates at the inhaler outlet.

Primary PSDs resulting from CFD-DPM simulations are depicted in Fig. 10. The presented data demonstrate differences between the predicted size distribution of particles leaving the inhaler for different test formulations. Cumulative distribution data (Fig. 10) were used to calculate the corresponding aerodynamic PSDs, and the derived MMAD and GSD values were compared with the values calculated from DPI PSD data measured using ACI (Fig. 9b,c). In general, the simulations indicated much lower MMAD in comparison to the values calculated based on ACI measurements. The largest divergence between the *in vitro* and *in silico*-based MMAD values was observed for JM1 and JM2 samples, but notable difference were seen for other samples, too. As discussed by Djokic et al. (2014), relatively large MMAD for JM1 and JM2 sample, calculated based on ACI analysis, may result from particle tendency to form aggregates. In addition, adhesion of particles to the

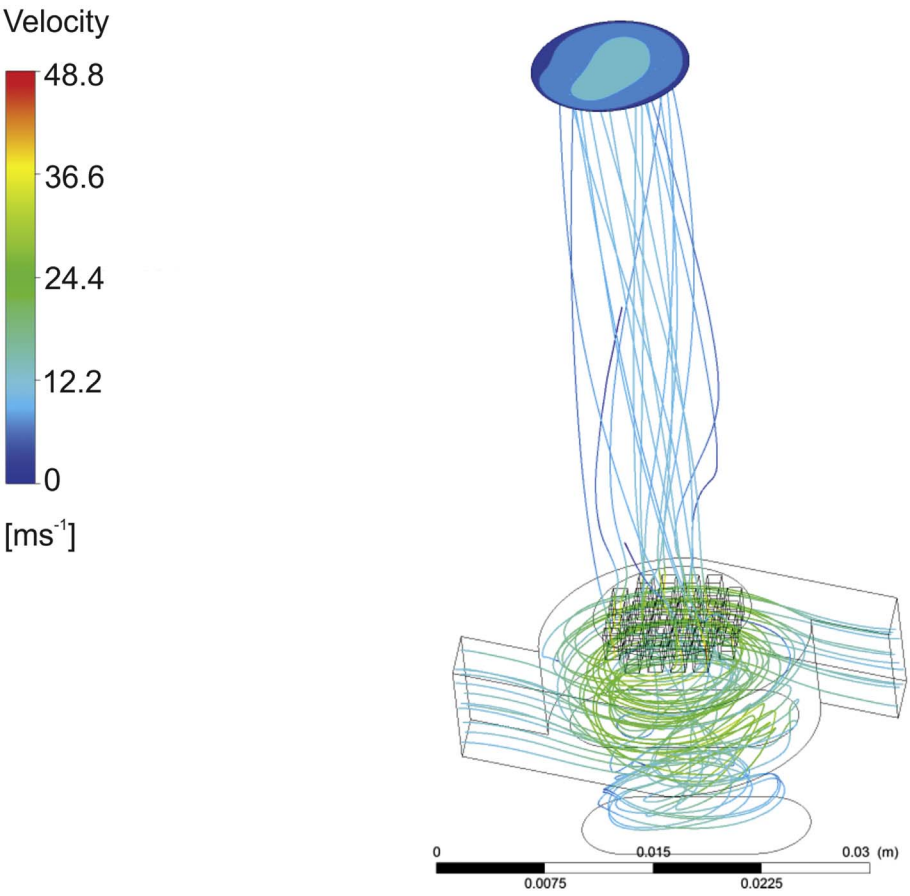

Fig. 7. Velocity streamlines (JM2) – isometric view.

impactor walls might also influence the obtained *in vitro* results (de Boer et al., 2002). Similar observations were made for GSD where CFD-DPM generated values indicated more narrow aerosol size distribution, specially in the case of JM1 and JM2 samples. These findings imply that the aerosol cloud that leaves the inhaler might contain smaller particles, with narrower size distribution, than assumed based on ACI measurements. Therefore, CFD-DPM generated results, in conjunction with the *in silico* model that describes particles transport through the lungs (*e.g.* ICRP66 model (ICRP, 1994)), can be used as an alternative to the *in vitro* ACI assessment of DPI deposition pattern *in vivo*. Still, we need to note that the described CFD-DPM approach may lead to an underestimation of MMAD when a significant portion of particles leaves the inhaler as agglomerates, which is often the case for DPIs. We should also note that the assumption of a 100% sticking efficiency of large particles or aggregates could contribute to the underestimation of MMAD as this would effectively eliminate the large particle sizes from the *in silico* predicted PSD. In order to accurately describe properties of the inhaled aerosols, simulation tools need to address complicated

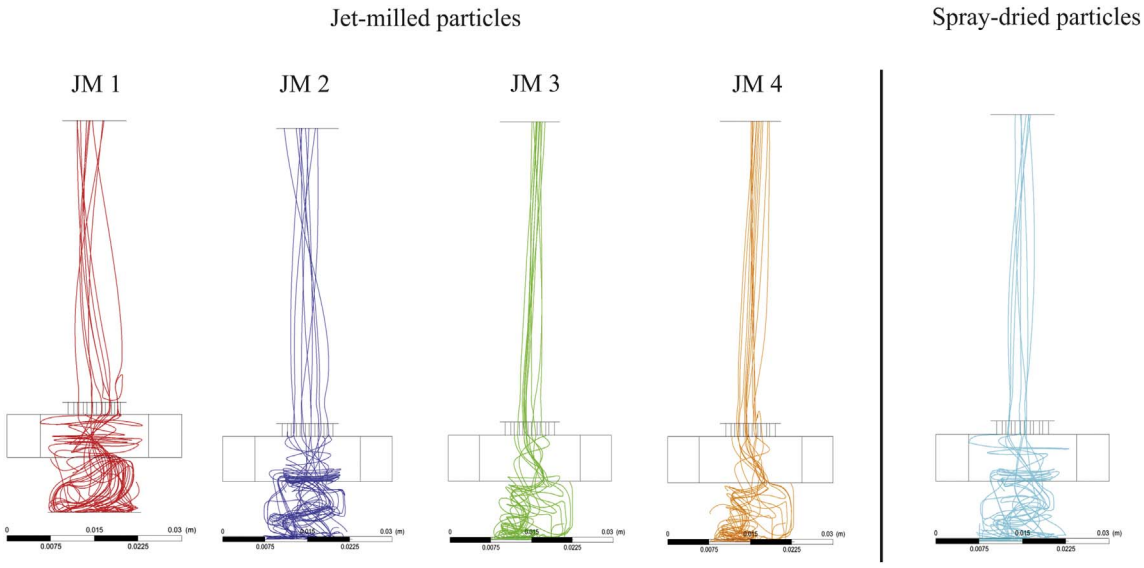

Fig. 8. Particle tracking from the beginning of the simulation to the outlet.

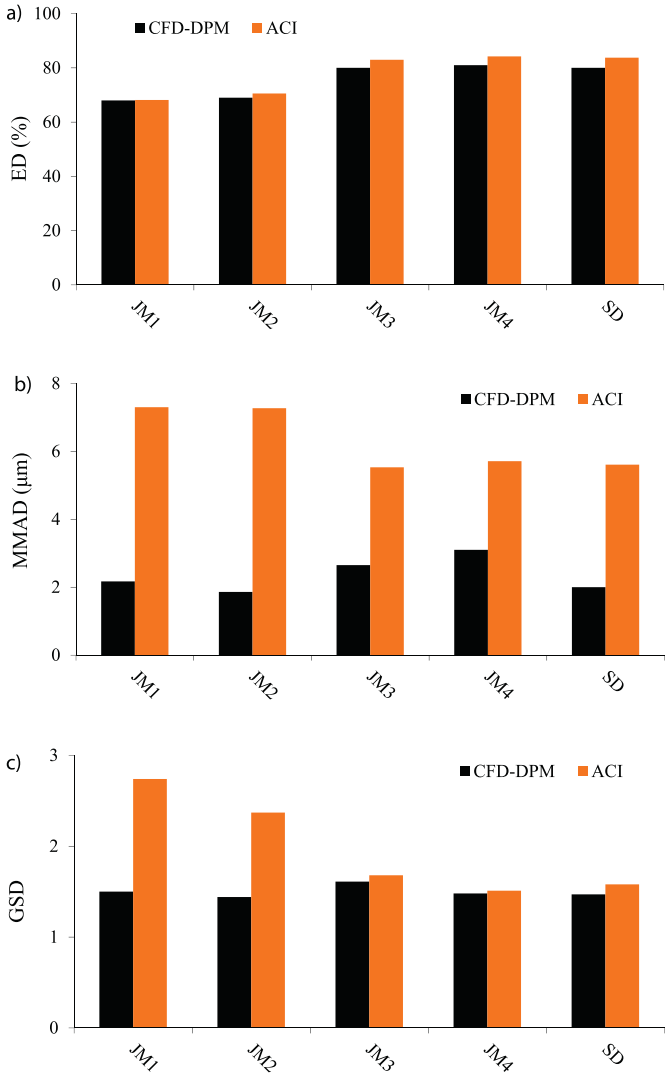

Fig. 9. Comparison of aerodynamic particle properties: ED (a), MMAD (b), and GSD (c) derived from CFD-DPM output data and ACI results taken from Djokic et al. (2014).

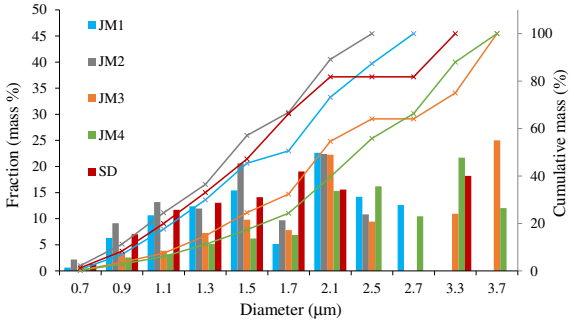

Fig. 10. Fractional and cumulative primary PSDs (geometric diameter) resulting from CFD-DPM simulations for five model formulations; values on x-scale denote the upper cut-off diameter.

particle-particle and particle-wall interactions, including agglomeration and de-agglomeration.

Fig. 11 shows CFD-DPM predicted percentage of deposited particles in different deposition sites (capsule chamber, circulation chamber, grid area and mouthpiece) for the corresponding Q = 28.3 l/min. The presented simulation results correspond to each of the powder types JM1-JM4 and SD. It can be observed that most particles deposit in either capsule or circulation chamber, while only a small percentage of particles deposit in the mouthpiece.

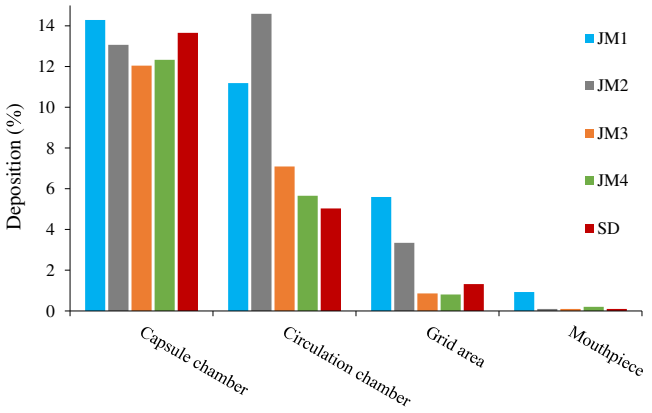

Fig. 11. Regional particle deposition in the Aerolizer. Q = 28.3 l/min.

3.4. PBPK model construction

After inhalation, amiloride enters the systemic circulation in two phases: quickly *via* respiratory tract, and more slowly following GI absorption of the swallowed part of the dose (Jones et al., 1997; Noone et al., 1997). Therefore, drug-specific PBPK model was first developed and validated for oral drug dosing, and further adjusted to simulate plasma profile following inhalation. A simpler compartmental model might also have been used for amiloride pharmacokinetic modelling, but a whole body PBPK was considered advantageous because of its wider applicability. Namely, it can be used in future studies to forecast drug-drug or drug-disease (in terms of physiological conditions) interactions.

The simulation results for 10 mg amiloride oral solution and 20 mg IR oral capsule are shown in Fig. 12 and Table 3. The two profiles were based on the same input data (Table 2), with the only differences concerning the selection of drug dose, dosage form, and concomitant simulation of drug dissolution from a capsule. Due to high solubility of amiloride HCl, the predicted drug dissolution from IR capsule happened almost immediately (100% drug dissolved in 5 min), which resulted in the same t_{max} for both formulations.

The predicted pharmacokinetic parameters for 10 mg amiloride oral dose fitted into the range of values reported in literature (Jones et al., 1997; Spahn et al., 1987). The simulation results for 20 mg drug dose also agreed with the *in vivo* data, as demonstrated by %PE values < 10% for t_{max} and AUC (Table 3). In this case, larger deviation from the mean *in vivo* data (Weiss et al., 1969) was noted solely for C_{max}, but

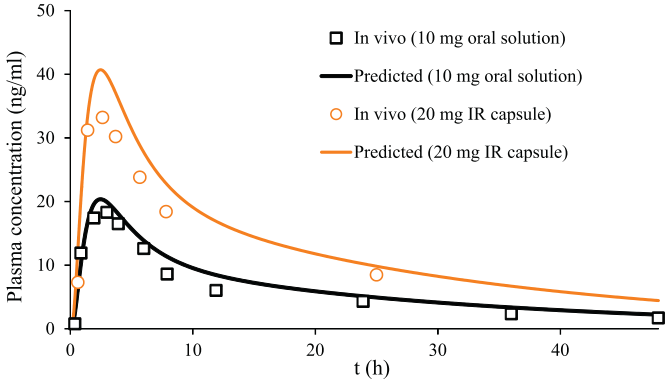

Fig. 12. Predicted amiloride plasma concentration-time profiles, along with the mean data observed in the *in vivo* studies for 10 mg oral solution (Jones et al., 1997) and 20 mg oral capsule (Weiss et al., 1969).

Table 3
Comparison of the predicted and observed pharmacokinetic parameters for 10 mg and 20 mg amiloride oral dose, and 1.91 mg delivered dose from a nebulized solution.

	Parameter	C_{max} (ng/ml)	t_{max} (h)	$AUC_{0-\infty}$ (ng h/ml)
10 mg oral solution	Predicted (%PE)	20.35 (− 11.20)	2.44 (18.39)	380.80 (− 17.66)
	In vivo mean[a]	18.30	2.99	323.64
	In vivo range[b]	9.80–30.60	1.90–4.40	160.00–390.00
20 mg IR capsule	Predicted (%PE)	40.70 (− 22.59)	2.44 (7.22)	761.58 (− 0.59)
	In vivo mean[c]	33.20	2.63	757.14
	In vivo range[d]	28.80–61.30	/	/
1.91 mg nebulized solution	Predicted M1 (%PE)	1.45 (− 9.02)	0.32 (38.46)	25.79 (− 46.45)
	Predicted M2 (%PE)	1.44 (− 8.27)	0.36 (30.77)	25.79 (− 46.45)
	Predicted M3 (%PE)	1.35 (− 1.50)	0.48 (7.69)	25.79 (− 46.45)
	Predicted M4 (%PE)	1.21 (9.02)	0.9 (− 73.08)	25.79 (− 46.45)
	In vivo mean[a]	1.33	0.52	17.61
	In vivo range[e]	0.10–3.20	0.30–0.70	3.20–32.00

[a] Refer to the mean plasma concentration–time profile from a single study (Jones et al., 1997).
[b] Refer to the range of values from different studies (Jones et al., 1997; Spahn et al., 1987).
[c] Refer to the mean plasma concentration–time profile from a single study (Weiss et al., 1969).
[d] Refer to the range of values from different studies (Weiss et al., 1969; Grayson et al., 1971).
[e] Refer to the range of values from a single study (Jones et al., 1997).

considering the range of values observed in different studies (Weiss et al., 1969; Grayson et al., 1971), the simulated value can be considered as a reasonable estimate. In addition, the estimated Vd value of 577.97 l agreed well with the large volume of distribution reported in literature (Grayson et al., 1971; Savic et al., 2007), and the predicted elimination half-life ($t_{1/2}$ = 16.02 h) matched the *in vivo* observed values (Jones et al., 1997; Spahn et al., 1987), indicating that the selected PBPK model parameters adequately describe amiloride pharmacokinetics.

In the next step, the generated model was adjusted to predict the absorption of a nebulized amiloride solution, at 1.91 mg dose level. This was the estimated dose delivered to the lungs, determined from the initial dose (4.5 mg) minus the amount of drug entrapped in the nebulizer (Jones et al., 1997). The additional adjustments in the model parameters included dosage form (pulmonary solution), and mean particle size (*in vitro* obtained MMAD = 4 μm taken from literature (Jones et al., 1997)). In addition, it was assumed that fraction of the inhaled drug (from extra-thoracic region) would be swallowed, and in order to match the *in vivo* data (Jones et al., 1997) gastric residence time was prolonged to 1 h to simulate the scenario where it takes some time for the swallowed portion of the drug to reach gastrointestinal tract.

The obtained results are presented in Fig. 13 and Table 3. Initial simulation (model M1) provided plausible prediction of the inhaled amiloride absorption. However, this model was based on the default

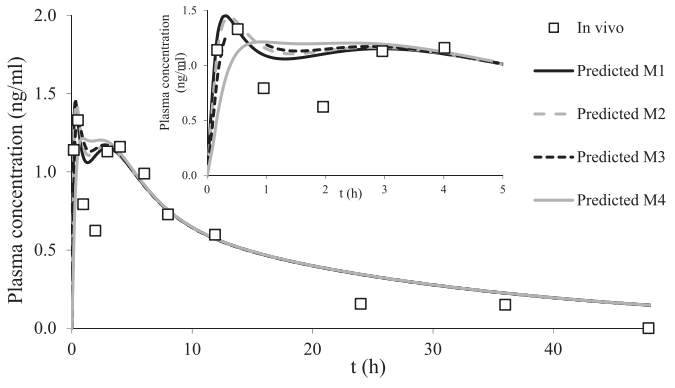

Fig. 13. Predicted amiloride plasma concentration-time profiles (M1-M4), along with the mean data observed in the *in vivo* study for 1.91 mg dose from the nebulized solution (Jones et al., 1997); M1 refers to the model using default $k_{a(p)}$, M2 refers to model using 25% reduced $K_{a(p)}$, M3 refers to model using 50% reduced $K_{a(p)}$, M4 refers to model using 75% reduced $K_{a(p)}$ in comparison to the default value; inset shows enlarged initial parts of the plasma concentration-time curves.

software calculated $K_{a(p)}$ for amiloride of 8.42 × 10^{-3} 1/s (under default settings, a uniform value is used for all pulmonary compartments), which may not be considered adequate in the case of a basic compound like this. Namely, default $K_{a(p)}$ is estimated from the lung volume, blood flow, drug tissue to plasma partition coefficient and blood to plasma concentration ratio (GastroPlus™ manual, 2015), and it does not take into account specific phenomena that may happen *in vivo*. Some recent studies, using a model based population pharmacokinetic approach or *in vitro* lung slice methodology, have demonstrated that certain basic drugs (*e.g.* olodaterol, some β2-sympathomimetics) exhibit prolonged pulmonary residence times due to lysosomal trapping in the lungs and thus delayed absorption (Backstrom et al., 2016; Borghardt et al., 2016). It was further noted in these reports that drug absorption from the lungs can be described as parallel absorption processes with different rate constants, whereas the initial fast absorption is responsible for the early C_{max}, while slow absorption (a major fraction) becomes apparent in the terminal phase and may contribute to the prolonged therapeutic effect. Furthermore, these different absorption processes can take place in the same lung region, *e.g.* fast and slow absorption from the alveolar space as demonstrated for the inhaled olodaterol (Borghardt et al., 2016), meaning that they could not be matched with distinct pulmonary compartments.

In order to assess the influence of decreased lung absorption rate on the generated pharmacokinetic profiles for amiloride, we have reduced the initial $K_{a(p)}$ values by 25% (model M2), 50% (model M3) and 75% (model M4). According to the obtained results, the reduction in $K_{a(p)}$ had no influence on the extent of amiloride absorption (the same predicted AUC values), but there were noticeable differences in the predicted C_{max}, and especially t_{max} values (Table 3). The best match between the *in vivo* and predicted data was observed with model M3, where the initial $K_{a(p)}$ was decreased by 50%. These results indicate that inhaled amiloride, similar to other basic drugs, exhibit certain delay in pulmonary absorption. Increasing the extent of $K_{a(p)}$ reduction leads to the loss of the early peak in plasma concentration-time profile, as demonstrated with the model M4 (Fig. 13). Therefore, model M3 was adopted for further exploration. It could still be speculated whether this model best describes inhaled amiloride pharmacokinetics because of the inability to interpret possible parallel (fast and slow) pulmonary absorption processes. Namely, in the current PCAT™ model only one $K_{a(p)}$ value can be ascribed to each pulmonary compartment. In this context, upgrades in the software PCAT™ model might improve *in silico* predictions for this drug.

According to the data in Table 3, the predictive ability of M3 model seems rather good. %PE for AUC, calculated based on mean *in vivo* data, was somewhat high; however, the predicted value fitted into the range

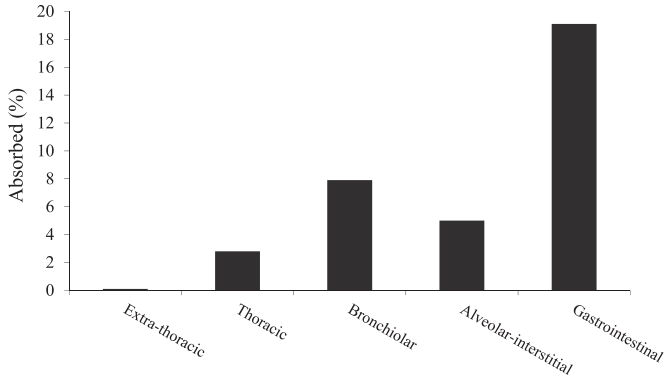

Fig. 14. Predicted regional absorption profile of amiloride following inhalation of a 1.91 mg dose from the nebulized solution.

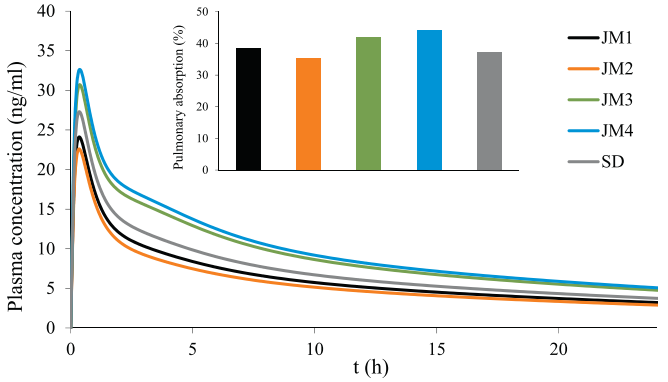

Fig. 16. Simulated drug plasma concentration-time profiles for different amiloride DPI formulations; inset shows percent of delivered dose absorbed through the lungs.

of individually recorded values (Jones et al., 1997). Moreover, certain deviations from the mean *in vivo* observed profile might be ascribed to the lack of adequate input data regarding PSD. Namely, the authors (Jones et al., 1997) only specified MMAD, and stated that the target site for this heterodispersed aerosol were the conducting airways. The predicted regional absorption distribution indicated that about half of the systemically available amiloride following inhalation of the nebulized solution is absorbed through the lungs (15.8%), while the rest of the dose is absorbed from the gastrointestinal tract (Fig. 14). These results are in accordance with the findings of Jones et al. (1997), demonstrating that the generated model M3 was able to interpret the absorption pattern of nebulized amiloride, including the second peak phenomenon.

3.5. PBPK model exploration

The constructed amiloride-specific absorption model (model M3) was consequently used to predict pulmonary deposition, and systemic drug absorption from different amiloride DPI experimental formulations. As already stated, these formulations had different aerodynamic properties, and relevant attributes (*i.e.*, CFD-DPM predicted delivered dose and particle size) were accounted for in the input parameters datasets. Aerodynamic PSD for each formulation, estimated based on CFD-DPM results, was used to forecast drug deposition through different pulmonary compartments. The simulated deposition profiles are depicted in Fig. 15. It can be noted that drug deposition fractions in peripheral region of the lungs will be similar for all formulations. More pronounced differences are seen in drug deposition in the conducting airways, whereas formulations with higher MMAD values (JM3 and JM4) will have higher percentage of drug deposited in these regions. In contrast, in the case of very small particles with MMADs $\leq 2\,\mu m$ (formulations JM1, JM2 and SD), > 50% of the delivered dose will be exhaled, under normal physiological conditions and breathing pattern as specified in the model.

The corresponding plasma concentration-time profiles for the five formulations are shown in Fig. 16, along with the data on pulmonary drug absorption. Since majority of inhaled amiloride is absorbed through the lung compartments (smaller portion is swallowed and absorbed from the gastrointestinal tract), extent of systemic drug bioavailability is a reflection of pulmonary absorption. In the case of JM1 and JM2, drug absorption is expected to be additionally decreased because aerosol delivery (in terms of delivered dose) is less efficient, as outlined in Fig. 9a.

As already mentioned, one of the benefits associated with PBPK modelling is prediction of drug absorption under different physiological conditions. Since cystic fibrosis is usually associated with impaired airflow (Zapletal et al., 1993), sensitivity analysis was run to investigate the effect of this parameter on the expected amiloride regional lung deposition. Simulated data for the formulation JM4, depicted in Fig. 17, illustrate how decreased airflow can decrease amiloride deposition in the conducting airways, which are the target site for this drug action. Such results suggest that drug & patient-specific PBPK modelling can provide quantitative data on the expected drug concentration in target site of the lungs, and thus enable the selection of appropriate dosing regimen.

4. Conclusion

The particle dispersion in a DPI was simulated by a CFD-DPM model. Boundary conditions that included velocity inlet and pressure outlet were set based on experiments of Djokic et al. (2014). Input data on particle characteristics were taken from the same study. For the corresponding turbulence model, k-ω model was used, and it was assumed that particles behave in such a way that in contact with wall they stay “trapped”, and the particles that reach the outlet surface “escape”

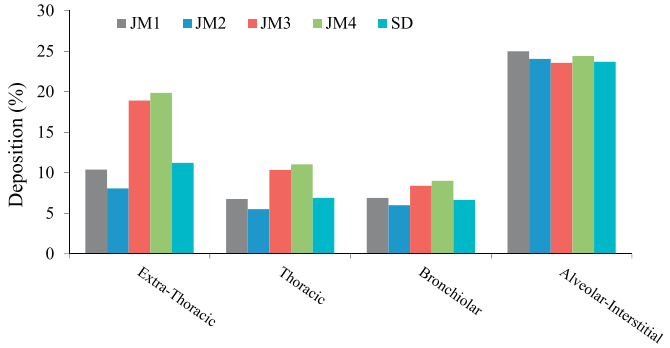

Fig. 15. Simulated lung deposition pattern of the inhaled amiloride particles from different formulations expressed as percent of delivered dose.

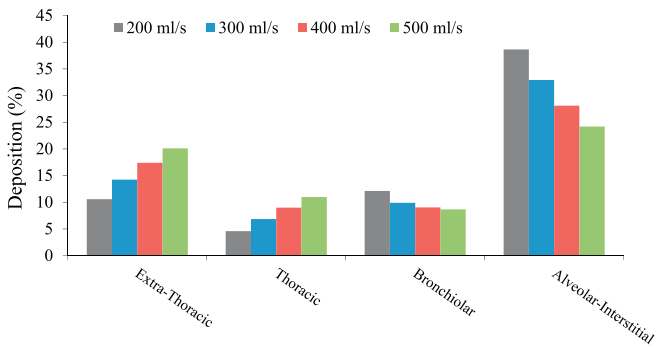

Fig. 17. The dependence of regional particle deposition (expressed as percent of delivered dose) on the variations in airflow rate.

the device domain. Under this assumption, it was possible to calculate how many particles were set at the beginning of the calculation, and how many particles got out of the device. Analysis of the flow field using CFD analysis provided information about air velocity during inhalation. Based on this flow field, we were able to determine how drug particles are moving from the capsule chamber until the end of the barrel, and particle distribution present on the outlet. The results indicate that particles mostly get "trapped" inside the carrier area because of the swirl flow, and this swirling flow becomes less dominant through the mouthpiece, as the tangential air inlets which introduce a swirl component, do not have such great impact down the flow after the grid structure. CFD-DPM generated values for the percent ED are within 4.5% difference compared to the experimental data obtained by Djokic et al. (2014). Results presented in the CFD-DPM part here are obtained with simplification that included only particles that were placed at the bottom of the chamber area and did not include the capsule itself. Also, the constructed model did not account for particle interactions such as agglomeration and de-agglomeration, and these phenomena will be included in the upgraded version of the model. Future work will include new simulations with inhaler where particles will be inside of a capsule, and the results will be used as input in the analysis that includes particle tracking inside patient's lungs.

Although computationally-intensive, this approach can be seen as useful alternative to *the in vitro* determination of aerosolized particle properties using ACI or other types of impactors. Linked with PBPK modelling, these data enable prediction of drug absorption in specific patients, under different physiological conditions, which may facilitate the decision on efficient dose levels for specific patients. The combined CFD-PBPK modelling might be seen as a promising tool in the design and characterization of DPIs; however, this approach needs to be additionally tested with different DPI types, and different model drugs.

Acknowledgements

This study is based upon work from COST Action MP1404 SimInhalle 'Simulation and pharmaceutical technologies for advanced patient-tailored inhaled medicines', supported by COST (European Cooperation in Science and Technology) www.cost.eu. In addition, this work was supported by the Ministry of Education, Science and Technological Development, Republic of Serbia with projects TR34007, III41007 and OI174028.

References

Agoram, B., Woltosz, W., Bolger, M., 2001. Predicting the impact of physiological and biochemical processes on oral drug bioavailability. Adv. Drug Deliv. Rev. 50, S41–S67.

Almukainzi, M., Jamali, F., Aghazadeh-Habashi, A., Löbenberg, R., 2016. Disease specific modeling: simulation of the pharmacokinetics of meloxicam and ibuprofen in disease state vs. healthy conditions. Eur. J. Pharm. Biopharm. 100, 77–84.

Alqahtani, S., Kaddoumi, A., 2016. Development of a physiologically based pharmacokinetic/pharmacodynamic model to predict the impact of genetic polymorphisms on the pharmacokinetics and pharmacodynamics represented by receptor/transporter occupancy of central nervous system drugs. Clin. Pharmacokinet. 55 (8), 957–969.

Backman, P., Tehler, U., Olsson, B., 2016. Predicting exposure after oral inhalation of the selective glucocorticoid receptor modulator, AZD5423, based on dose, deposition pattern, and mechanistic modelling of pulmonary disposition. J. Aerosol Med. Pulm. Drug Deliv. 30 (2), 108–117.

Backstrom, E., Boger, E., Lundqvist, A., Hammarlund-Udenaes, M., Friden, M., 2016. Lung retention by lysosomal trapping of inhaled drugs can be predicted in vitro with lung slices. J. Pharm. Sci. 105 (11), 3432–3439.

de Boer, A.H., Gjaltema, D., Hagedoorn, P., Frijlink, H.W., 2002. Characterization of inhalation aerosols: a critical evaluation of cascade impactor analysis and laser diffraction technique. Int. J. Pharm. 249 (1–2), 219–231.

Borghardt, J.M., Weber, B., Staab, A., Kloft, C., 2015. Pharmacometric models for characterizing the pharmacokinetics of orally inhaled drugs. AAPS J. 17 (4), 853–870.

Borghardt, J.M., Weber, B., Staab, A., Kunz, C., Formella, S., Kloft, C., 2016. Investigating pulmonary and systemic pharmacokinetics of inhaled olodaterol in healthy volunteers using a population pharmacokinetic approach. Br. J. Clin. Pharmacol. 81 (3), 538–552.

Bouzom, F., Ball, K., Perdaems, N., Walther, B., 2012. Physiologically based pharmacokinetic (PBPK) modelling tools: how to fit with our needs? Biopharm. Drug Dispos. 33 (2), 55–71.

Brocklebank, D., Ram, F., Wright, J., Barry, P., Cates, C., Davies, L., Douglas, G., Muers, M., Smith, D., White, J., 2001. Comparison of effectiveness of inhaler devices in asthma and chronic obstructive airway disease: a systematic review of the literature. Health Technol. Assess. 5 (26), 1–149.

Chan, H.K., 2006. Dry powder aerosol delivery systems: current and future research directions. J. Aerosol Med. 19 (1), 21–27.

Chaudhuri, S.R., Lukacova, V., 2010. Simulating delivery of pulmonary (and intranasal) aerosolised drugs. Orally Inhaled Nasal Drug Prod. 26–30.

Chetty, M., Rose, R.H., Abduljalil, K., Patel, N., Lu, G., Cain, T., Jamei, M., Rostami-Hodjegan, A., 2014. Applications of linking PBPK and PD models to predict the impact of genotypic variability, formulation differences, differences in target binding capacity and target site drug concentrations on drug responses and variability. Front. Pharmacol. 5, 258.

Christopher, J.D., Dey, M., Lyapustina, S., Mitchell, J.P., Tougas, T.P., Van Oort, M., Strickland, H., Wyka, B., 2010. Generalized simplified approaches for mass median aerodynamic determination. Pharmacopeial Forum. 36 (3), 812–823.

Clark, A.R., 2004. Pulmonary delivery technology: recent advances and potential for the new millennium. In: Hickey, A.J. (Ed.), Drugs and the Pharmaceutical Sciences. Marcel Dekker, Inc., New York, pp. 571–591.

Coates, M.S., Fletcher, D.F., Chan, H.K., Raper, J.A., 2004. Effect of design on the performance of a dry powder inhaler using computational fluid dynamics. Part 1: grid structure and mouthpiece length. J. Pharm. Sci. 93 (11), 2863–2876.

Coates, M.S., Chan, H.-K., Fletcher, D.F., Raper, J.A., 2005a. Influence of air flow on the performance of a dry powder inhaler using computational and experimental analyses. Pharm. Res. 22 (9), 1445–1453.

Coates, M.S., Fletcher, D.F., Chan, H.-K., Raper, J.A., 2005b. The role of capsule on the performance of a dry powder inhaler using computational and experimental analyses. Pharm. Res. 22 (6), 923–932.

Coates, M.S., Chan, H.-K., Fletcher, D.F., Raper, J.A., 2006. Effect of design on the performance of a dry powder inhaler using computational fluid dynamics. Part 2: air inlet size. J. Pharm. Sci. 95 (6), 1382–1392.

Coates, M.S., Chan, H.K., Fletcher, D.F., Chiou, H., 2007. Influence of mouthpiece geometry on the aerosol delivery performance of a dry powder inhaler. Pharm. Res. 24 (8), 1450–1456.

Dahlgren, D., Roos, C., Sjögren, E., Lennernäs, H., 2015. Direct in vivo human intestinal permeability (Peff) determined with different clinical perfusion and intubation methods. J. Pharm. Sci. 104 (9), 2702–2726.

Djokic, M., Kachrimanis, K., Solomun, Lj, Djuris, J., Vasiljevic, D., Ibric, S., 2014. A study of jet-milling and spray-drying process for the physicochemical and aerodynamic dispersion properties of amiloride HCl. Powder Technol. 262, 170–176.

Fagerholm, U., 2007. Prediction of human pharmacokinetics — renal metabolic and excretion clearance. J. Pharm. Pharmacol. 59 (11), 1463–1471.

Feng, Y., Kleinstreuer, C., 2014. Micron-particle transport, interactions and deposition in triple lung-airway bifurcations using a novel modelling approach. J. Aerosol Sci. 71, 1–15.

Fröhlich, E., Mercuri, A., Wu, S., Salar-Behzadi, S., 2016. Measurements of deposition, lung surface area and lung fluid for simulation of inhaled compounds. Front. Pharmacol. 7, 181.

GastroPlus™ version 9.0 Manual, 2015. SimulationPlus Inc., Lancaster.

Ghalichi, F., Deng, X., Champlain, A.D., Douville, Y., King, M., Guidoin, R., 1998. Low Reynolds number turbulence modelling of blood flow in arterial stenoses. Biorheology 35 (4–5), 281–294.

Grayson, M.F., Smith, A.J., Smith, R.N., 1971. Absorption, distribution and elimination of 14 C-amiloride in normal human subjects. Br. J. Pharmacol. 43 (2), 473P–474P.

Hoppentocht, M., Hagedoorn, P., Frijlink, H.W., de Boer, A.H., 2014. Technological and practical challenges of dry powder inhalers and formulations. Adv. Drug Deliv. Rev. 75, 18–31.

ICH, 2005. ICH Harmonised Tripartite Guideline Pharmaceutical Development Q8 (R2), Current Step 4 Version. https://www.ich.org/fileadmin/Public_Web_Site/ICH_Products/Guidelines/Quality/Q8_R1/Step4/Q8_R2_Guideline.pdf, Accessed date: 31 March 2017.

ICRP, 1994. Human Respiratory Tract Model for Radiological Protection. ICRP Publication 66. Ann. ICRP 24, pp. 1–3.

IPCS INCHEM Amiloride Hydrochloride (Monograph 026). http://www.inchem.org/documents/pims/pharm/pim026.htm, Accessed date: 4 July 2017.

Islam, N., Gladki, E., 2008. Dry powder inhalers (DPIs) — a review of device reliability and innovation. Int. J. Pharm. 360 (1–2), 1–11.

Jiang, L., Tang, Y., Zhang, H., Lu, X., Chen, X., Zhu, J., 2012. Importance of powder residence time for the aerosol delivery performance of a commercial dry powder inhaler Aerolizer®. J. Aerosol Med. Pulm. Drug Deliv. 25 (5), 265–279.

Jones, H., Rowland-Yeo, K., 2013. Basic concepts in physiologically based pharmacokinetic modeling in drug discovery and development. CPT Pharmacometrics Syst. Pharmacol. 2 (e63).

Jones, K.M., Liao, E., Hohneker, K., Turpin, S., Henry, M.M., Selinger, K., Hsyu, P.H., Boucher, R.C., Knowles, M.R., Dukes, G.E., 1997. Pharmacokinetics of amiloride after inhalation and oral administration in adolescents and adults with cystic fibrosis. Pharmacotherapy 17 (2), 263–270.

Kleinstreuer, C., Shi, H., Zhang, Z., 2007. Computational analyses of a pressurized metered dose inhaler and a new drug–aerosol targeting methodology. J. Aerosol Med. 20 (3), 294–309.

Kleinstreuer, C., Feng, Y., Childress, E., 2014. Drug-targeting methodologies with applications: a review. World J. Clin. Cases 2 (12), 742–756.

Kloss, C., Goniva, C., Aichinger, G., Pirker, S., 2009. Comprehensive DEM-DPM-CFD simulations — model synthesis, experimental validation and scalability. In: Seventh International Conference on CFD in the Minerals and Process Industries; CSIRO,

Melbourne, Australia, December 9–11.
Kostewicz, E.S., Aarons, L., Bergstrand, M., Bolger, M.B., Galetin, A., Hatley, O., Jamei, M., Lloyd, R., Pepin, X., Rostami-Hodjegan, A., Sjögren, E., Tannergren, C., Turner, D.B., Wagner, C., Weitschies, W., Dressman, J., 2014. PBPK models for the prediction of in vivo performance of oral dosage forms. Eur. J. Pharm. Sci. 57, 300–321.
Launder, B.E., Spalding, D., 1974. The numerical computation of turbulent flows. Comput. Methods Appl. Mech. Eng. 3 (2), 269–289.
Li, A., Ahmadi, G., 1992. Dispersion and deposition of spherical particles from point sources in a turbulent channel flow. Aerosol Sci. Technol. 16 (4), 209–226.
Longest, P.W., Holbrook, L.T., 2012. In silico models of aerosol delivery to the respiratory tract — development and applications. Adv. Drug Deliv. Rev. 64 (4), 296–311.
Longest, P.W., Hindle, M., Choudhuri, S.D., Byron, P.R., 2007. Numerical simulations of capillary aerosol generation: CFD model development and comparisons with experimental data. Aerosol Sci. Technol. 41 (10), 952–973.
Longest, P.W., Hindle, M., Choudhuri, S.D., Xi, J., 2008. Comparison of ambient and spray aerosol deposition in a standard induction port and more realistic mouth–throat geometry. J. Aerosol Sci. 39 (7), 572–591.
Longest, P.W., Hindle, M., Choudhuri, S.D., 2009. Effects of generation time on spray aerosol transport and deposition in models of the mouth–throat geometry. J. Aerosol Med. Pulm. D 22 (2), 67–84.
Longest, P.W., Son, Y.J., Holbrook, L., Hindle, M., 2013. Aerodynamic factors responsible for the deaggregation of carrier-free drug powders to form micrometer and submicrometer aerosols. Pharm. Res. 30 (6), 1608–1627.
Lukacova, V., Parrott, N., Lave, T., Fraczkiewicz, M., Bolger, M., Woltosz, W., 2008. General approach to calculation of tissue:plasma partition coefficients for physiologically based pharmacokinetic (PBPK) modelling. AAPS National Meeting, Atlanta, November 15–20.
Menter, F.R., 1994. Two-equation eddy–viscosity turbulence models for engineering applications. AIAA J. 32 (8), 1598–1616.
Milenkovic, J., Alexopoulos, A.H., Kiparissides, C., 2013. Flow and particle deposition in the Turbuhaler: a CFD simulation. Int. J. Pharm. 448 (1), 205–213.
Milenkovic, J., Alexopoulos, A.H., Kiparissides, C., 2014a. Airflow and Particle Deposition in a Dry Powder Inhaler: An Integrated CFD Approach. Simulation and Modeling Methodologies, Technologies and Applications. Springer International Publishing, pp. 127–140.
Milenkovic, J., Alexopoulos, A.H., Kiparissides, C., 2014b. Deposition and fine particle production during dynamic flow in a dry powder inhaler: a CFD approach. Int. J. Pharm. 461 (1–2), 129–136.
Mitchell, J.P., Nagel, M.W., 2003. Cascade impactors for the size characterization of aerosols from medical inhalers: their uses and limitations. J. Aerosol Med. 16 (4), 341–377.
Mossaad, D.M.R., 2014. Drug delivery to the respiratory tract using dry powder inhalers. In: Electronic Thesis and Dissertation Repository, Paper 2036.
Noone, P.G., Regnis, J.A., Liu, X., Brouwer, K.L., Robinson, M., Edwards, L., Knowles, M.R., 1997. Airway deposition and clearance and systemic pharmacokinetics of amiloride following aerosolization with an ultrasonic nebulizer to normal airways. Chest 112 (5), 1283–1290.
Peters, S.A., 2008. Identification of intestinal loss of a drug through physiologically based pharmacokinetic simulation of plasma concentration-time profiles. Clin. Pharmacokinet. 47 (4), 245–259.
Samant, T.S., Lukacova, V., Schmidt, S., 2017. Development and qualification of physiologically based pharmacokinetic models for drugs with atypical distribution behavior: a desipramine case study. CPT Pharmacometrics Syst. Pharmacol. 6 (5), 315–321.
Sarfraz, M., Macwan, J., Almukainzi, M., Bolger, M., Loebenberg, R., 2015. The importance of lysosomal trapping for setting clinically relevant product specifications for dextromethorphan immediate release dosage forms. In: AAPS Annual Meeting and Exposition, Orlando, October 25–29.
Savic, R.M., Jonker, D.M., Kerbusch, T., Karlsson, M.O., 2007. Implementation of a transit compartment model for describing drug absorption in pharmacokinetic studies. J. Pharmacokinet. Pharmacodyn. 34 (5), 711–726.
Shur, J., Lee, S., Adams, W., Lionberger, R., Tibbatts, J., Price, R., 2012. Effect of device design on the in vitro performance and comparability for capsule-based dry powder inhalers. AAPS J. 14 (4), 667–676.
Sommerfeld, M., van Wachem, B., Oliemans, R., 2008. Best practice guidelines for computational fluid dynamics of dispersed multiphase flows. In: ERCOFTAC European Research Community on Flow, Turbulence and Combustion.
Spahn, H., Reuter, K., Mutschler, E., Gerok, W., Knauf, H., 1987. Pharmacokinetics of amiloride in renal and hepatic disease. Eur. J. Clin. Pharmacol. 33 (5), 493–498.
Strickland, H., Morgan, B., Mitchel, J.P., 2013. Physical causes of APSD changes in aerosols from OIPs and their impact on CI measurements. In: Tougas, T.P., Mitchel, J.P., Lyapustina, S.A. (Eds.), Good Cascade Impactor Practices, AIM and EDA for Orally Inhaled Products. Springer, New York, pp. 65–66.
Suri, A., Chapel, S., Lu, C., Venkatakrishnan, K., 2015. Physiologically based and population PK modeling in optimizing drug development: a predict-learn-confirm analysis. Clin. Pharmacol. Ther. 98 (3), 336–344.
Terzano, C., 2008. Dry powder inhaler and the risk of error. Respiration 75 (1), 14–15.
Theil, F.P., Guentert, T.W., Haddad, S., Poulin, P., 2003. Utility of physiologically based pharmacokinetic models to drug development and rational drug discovery candidate selection. Toxicol. Lett. 138 (1–2), 29–49.
Tong, Z.B., Zheng, B., Yang, R.Y., Yu, A.B., Chan, H.K., 2013. CFD-DEM investigation of the dispersion mechanisms in commercial dry powder inhalers. Powder Technol. 240, 19–24.
Tong, Z.B., Kamiya, H., Yu, A.B., Chan, H.K., Yang, R.Y., 2015. Multi-scale modelling of powder dispersion in a carrier-based inhalation system. Pharm. Res. 32 (6), 2086–2096.
Versteeg, H.K., Hargrave, G., Harrington, L., Shrubb, I., Hodson, D., 2000. The use of computational fluid dynamics (CFD) to predict pMDI air flows and aerosol plume formation. Respir. Drug Deliv. VII 1, 257–264.
Voss, A., Finlay, W.H., 2002. Deagglomeration of dry powder pharmaceutical aerosols. Int. J. Pharm. 248 (1–2), 39–50.
Weiss, P., Hersey, R.M., Dujovne, C.A., Bianchine, J.R., 1969. The metabolism of amiloride hydrochloride in man. Clin. Pharmacol. Ther. 10 (3), 401–406.
Wong, W., Fletcher, D.F., Traini, D., Chan, H.K., Young, P.M., 2012. The use of computational approaches in inhaler development. Adv. Drug Deliv. Rev. 64 (4), 312–322.
Wu, S., Salar-Behzadi, S., Fröhlich, E., 2013. Role of in-silico modelling in drug development for inhalation treatment. J. Mol. Pharm. Org. Process Res. 1 (2), 106.
Wu, S., Zellnitz, S., Mercuri, A., Salar-Behzadi, S., Bresciani, M., Fröhlich, E., 2016. An in vitro and in silico study of the impact of engineered surface modifications on drug detachment from model carriers. Int. J. Pharm. 513 (1–2), 109–117.
Zapletal, A., Desmond, K.J., Demizio, D., Coates, A.L., 1993. Lung recoil and the determination of airflow limitation in cystic fibrosis and asthma. Pediatr. Pulmonol. 15 (1), 13–18.
Zhou, Q., Tong, Z., Tang, P., Yang, R., Chan, H.K., 2013, June. CFD analysis of the aerosolization of carrier-based dry powder inhaler formulations. In: Yu, A., Dong, K., Yang, R., Luding, S. (Eds.), AIP Conference Proceedings. 1542(1). pp. 1146–1149.
Zhou, D., Bui, K., Sostek, M., Al-Huniti, N., 2016. Simulation and prediction of the drug-drug interaction potential of naloxegol by physiologically based pharmacokinetic modeling. CPT Pharmacometrics Syst. Pharmacol. 5 (5), 250–257.
Zhu, C., Jiang, L., Chen, T.M., Hwang, K.K., 2002. A comparative study of artificial membrane permeability assay for high throughput profiling of drug absorption potential. Eur. J. Med. Chem. 37 (5), 399–407.
Zhuang, X., Lu, C., 2016. PBPK modeling and simulation in drug research and development. Acta Pharm. Sin. B 6 (5), 430–440.